DRAFT

Ce rete Composi 7 (2019) 1

Contents l s availa at S enceDir

Cement and Concrete Composites

journal homepage: www.elsevier.com/locate/cemconcomp

Three-dimensional shape characterization of fine sands and the influence of particle shape on the packing and workability of mortars☆

Pierre Estephane[a,*], Edward J. Garboczi[b], Jeffrey W. Bullard[c], Olafur H. Wallevik[d]

[a] GCP Applied Technologies, 5006, Dubai, United Arab Emirates
[b] Na f Standards an er, CO, 80305, U States
[c] Na al Institute o dards an chnology, Gai burg, MD, 208 ted States
[d] IC eocenter, Reykj Univers & Innovation Ce Iceland, Arl 2, 112, Reykjav celand

DRAFT

ARTICLE INF

Key
Mortar
Sand
Workability
Sand shape
Packing
Tomography
Spherical harmonics

AB

Th aper studies a ction fine sands, their particle s pe and its effect on the plastic properties of mortars via the influence on the workability and packing of cementitious mixtures. Five sands from different sources were sampled, wet sieved, and classified into six size classes: 20 μm–75 μm, 75 μm–150 μm, 150 μm–300 μm, 300 μm–600 μm, 600 μm to 1.18 mm and 1.18 mm–2.36 mm. Particle shape was measured and various geometrical quantities were determined for particles of each class using a combination of X-ray microcomputed tomography (μCT) and spherical harmonic analysis. Specimen preparation, scanning method, minimum required number of particles in a representative sample, and shape histograms are all discussed, and used to classify and compare the shape of the particles of each material type and size class. This information is then used to establish a connection between sand particle shape and the wet packing density, the workability in the form of slump-flow, and the water demand in mortar mixtures.

1. Introduction

Concrete, as a main material for construction, is immensely important and has gone through many phases of technical development. It has been improved in terms of quality and suitability in response to the continuously increasing demands of technical specifications, especially in urban environments. High-rise buildings, long bridges, decorative detailing, and textured and colourfully shaped building elements are frequent projects where complicated technical conditions like long continuous concrete pours, high pour rates, and adequate pumpability are required [1,2]. These requirements can be satisfied by making sure that the concrete in its fresh state has the appropriate rheological behaviour and properties [3]. It has been shown that the shape of aggregates greatly influence the workability of concrete and its rheological properties [4], and fine crushed aggregates can greatly influence the rheology of self-compacting concrete [5]. The magnitude of these effects depends on the type of concrete and application. Due to the influence of aggregate quality on rheology, their scarcity as a result of increasing urbanization and environmental constraints on their extraction [6], and the possible presence of mineral contaminants [7,8], it is imperative to examine available aggregates and their properties to understand their suitability for different types of applications. This analysis can result in a procedure to rate the aggregate characteristics needed to fulfil concrete rheological requirements.

Previous work has shown the influence of coarse and fine aggregates, microfine aggregates, and even finer fillers on the rheological behaviour of concrete [4,5,9–13]. It was also shown how a higher packing density can reduce the volume of voids between adjacent particles and increase the ability of the paste to sufficiently fill up these voids for an improved lubrication of the particles and consequently higher workability and flowability of the mortar or concrete [39]. The porosity and permeability of concrete are as well reduced with the optimized particle packing, which will improve the overall durability of building elements [30]. This present paper focuses on the importance of the geometrical and shape metrics of particles with a size defined by sieving between 20 μm and 2.36 mm, which covers the range of what is usually called sand or fine aggregates and microfine aggregates. Sand particles from different sources and shapes were proportioned based on clearly defined mix designs and assessed for their performance in cementitious suspensions when compared to the rounded particles of a CEN (Comité Européen de Normalisation: European Committee for Standardization) standard sand [14]. These rounded particles were

☆ Partial contribution of NIST, not subject to US copyright.

* Corresponding author.
E-mail address: pierre.estephane@gcpat.com (P. Estephane).

https://doi.org/10.1016/j.cemconcomp.2018.12.018
Received 1 August 2018; Received in revised form 26 November 2018; Accepted 23 December 2018
Available online 25 December 2018
0958-9465/ © 2018 Elsevier Ltd. All rights reserved.

taken as a reference due to their tendency to have a maximum geometrical packing density [15–19] as well as for facilitated mobility, reduced friction, and lower resistance to flow in suspension [20].

Five samples of different types and sources of sand were collected within the United Arab Emirates, and compared to the CEN standard sand. Such types of sand are familiar in the ready-mix industry and used for all concrete applications. In total, six different sands were studied as received and were subject to descriptive petrographic examination and quantitative X-ray diffraction (QXRD). Each sand type was washed and sieved, and then classified into six size classes: 20 μm–75 μm, 75 μm–150 μm, 150 μm–300 μm, 300 μm–600 μm, 600 μm to 1.18 mm, and 1.18 mm–2.36 mm [21] using standard wire-mesh sieves with square openings. The particles in each class were analysed for their shape by X-ray microcomputed tomography (μCT) and spherical harmonic series [22].

The particles of the same type of sand were proportionally mixed following two different designs, W600 and W2360. W600 particles were tested for particle size distribution and other physical properties. W2360 particles were checked for physical properties and used in mortar tests to study their impact on wet packing density, workability, and water demand. The effect of particle shape on the workability of mortars concerning slump-flow (workability) will be shown, as well as which sand fraction was most influential on the wet packing density, using only the W2360 mixture design, defined in section 2.2.2.

A pertinent question concerning particle shape characterization is this: What is the minimum number of particles needed to adequately represent the real particle collection? In the course of this study, the minimum number of particles scanned by μCT that was needed to obtain representative shape distributions is discussed.

2. Experimental

2.1. Materials

The cement used in all experiments was an ordinary Portland cement, denoted CEM I 42.5R (EN 197-1). Its characteristics are shown in Table 1. The particle size distribution was measured by laser diffraction with a d_{50} value of 18.0 μm for the CEM I 42.5R, where N is the mass percentage of particles with laser diffraction-measured diameters less than or equal to d_N.

The reference sand used for all the mortar tests was a CEN standard sand, having naturally equant, rounded, clean, and a particle gradation according to BS EN 196-1 [14]. Its lithology was mainly quartz. Table 2 refers to the standard sand used. All percentages are mass percent.

Five more samples of sand of different types and sources were collected from the United Arab Emirates, with four from the Fujairah area (Sands # 1 to # 4) and one sample of dune sand from the Al Ain area (Sand # 5). The locations of these five sources of sand are shown in the map in Fig. 1 – see caption for color key.

Sands #1 to #4 were quarried as rocks then crushed to sand size. All these four sands were prepared following the same process: drilling and blasting, feeding to crushers, and screening and piling according to particle size. There were some differences. Sand 2 was produced using a vertical shaft impactor, while Sand 3 was prepared using a horizontal shaft impactor. Double deck screens and dust collectors were available in all plants. Sand 5 was collected as sand grains and not processed further in any way. All six types of sand were analysed for gradation following ASTM C136 [23].

Table 1
Phase composition (mass %) by QXRD and nitrogen BET surface area of CEM I (Bmill = Brownmillerite; C3A_c = C3A_cubic; C3A_o = C3A_ortho; Hemihyd = Hemihydrate).

Phase	CEM I	Phase	CEM I
Alite	58.9	Calcite	6.3
Belite	14.4	Gypsum	0.6
Bmill	5.2	Hemihyd	2.5
C3A_c	5.9	Anhydrite	2.6
C3A_o	2.3	Total SO3	3.5
Lime	0	BET SA (m^2/g)	0.936

Table 2
Sieve analysis of standard sand.

Sieve	Retained	Sieve	Retained
2.36 mm	0.0%	150 μm	20.3%
1.18 mm	27.7%	75 μm	7.7%
600 μm	35.3%	20 μm	0.3%
300 μm	8.7%		

Fig. 2 and Table 3 present the particle size distribution of the six types of sand as received and after elimination of the coarser portions retained on the 2.36 mm sieve. The same table demonstrates large differences of mass percentage passing of particles at the same sieve size. For example, for the 150 μm sieve, the range of mass percentage passing was between 4.0% and 16.0%. Because of this variation, any attempt to assess and compare the rheological behaviour of the six types of sand in mortar before standardization of the particle gradation would not be useful. This led to the necessity of segregating and proportioning the particles.

Wet sieving was practised on all types and sizes of sand according to BS 812–103.1 [21] eliminating the very fine materials and impurities that may coat the surface and thereby increase the water absorption of the sand particles. The washing was followed by oven drying at 105 °C. The obtained particles were cleaned and classified into six size classes: 20 μm–75 μm, 75 μm–150 μm, 150 μm–300 μm, 300 μm–600 μm, 600 μm to 1.18 mm and 1.18 mm–2.36 mm.

2.2. Testing and equipment

2.2.1. X-ray microcomputed tomography (μCT)

Particles from each type and class were shape characterized using a combination of X-ray microcomputed tomography (μCT) and spherical harmonic analysis [24,25]. Sand particles were embedded in epoxy resin at about 5% concentration by volume. Using a small vacuum pump, this mixture was pulled into plastic tubes having internal diameters of 4 mm, 6 mm, or 8 mm depending on the size of the particles to be scanned. The tube size was chosen so that its diameter was at least five times the size of the maximum-size particle embedded in the tube. Once hardened, the specimens showed suitable contrast between the sufficiently separated sand particles and the surrounding matrix because of the difference in the X-ray absorption characteristics between the epoxy matrix and the sand grains. These specimens were mechanically stable, being able to withstand transportation and rotation for several hours during scanning.

A selection of tubes was scanned, generating 2-D cross-sectional slices and then stacking them into 3-D representations. Various standard image analysis algorithms were used to separate particles that might have still been touching. The centre of mass of a particle was identified and taken as the origin to describe the particle by the function r (θ, ϕ) [24], where r is the distance from the centre of mass to the surface of a particle, in the direction defined by θ, ϕ, the spherical polar coordinate angles. This function is expanded in spherical harmonic functions, so that the shape of a particle, at the resolution of the original X-ray CT scan, is completely defined by a collection of 200–500 complex coefficients for each particle. The software gives each such particle a unique numerical label and automatically generates an image of the original voxel collection defining the particle from the X-ray scan as well as a smoother image generated from the spherical harmonic expansion, which are also referred to by the same numerical label but a different file name/format.

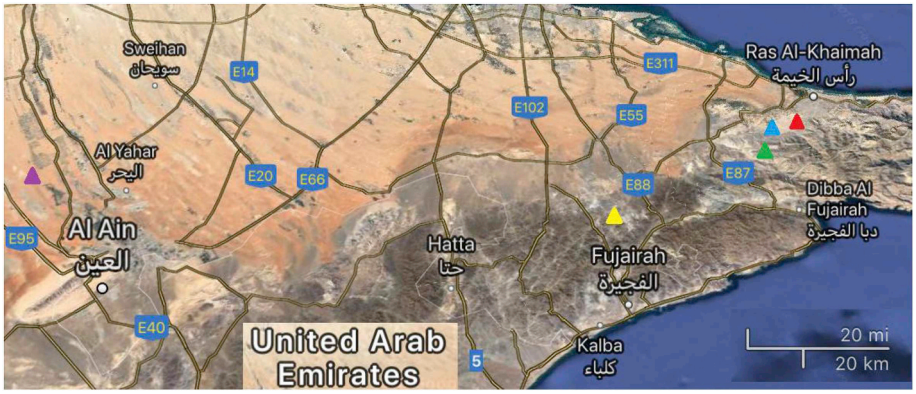

Fig. 1. Sampling locations of sand (red-Sand 1, blue-Sand 2, green-Sand 3, yellow-Sand 4, purple-Sand 5) (www.maps.google.com). (For interpretation of the references to colour in this figure legend, the reader is referred to the Web version of this article.)

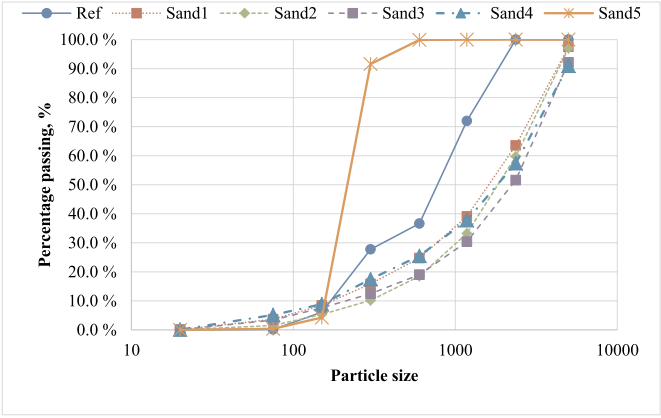

Fig. 2. Particle size distribution (horizontal axis in micrometers, using a logarithmic scale); for the six types of sand as received.

Table 3
Particle size distribution in form of mass percentage passing for the six types of sand after elimination of coarser portions.

Sieve size	Standard CEN	Sand 1	Sand 2	Sand 3	Sand 4	Sand 5
1.18 mm	71.96%	61.49%	55.62%	58.85%	65.82%	99.97%
600 µm	36.62%	38.97%	30.95%	36.87%	44.38%	99.89%
300 µm	27.74%	24.93%	17.05%	24.12%	30.41%	91.60%
150 µm	6.11%	13.30%	8.90%	14.70%	15.45%	4.23%
75 µm	0.12%	5.82%	2.54%	6.52%	8.94%	0.36%
20 µm	0.00%	0.06%	0.03%	0.12%	0.18%	0.00%

Further mathematical analysis of the particle can be carried out, since the spherical harmonic expansion allows for almost any surface or volume integral to be performed. Many metrics that characterize the shape of a particle are computed. These metrics included the length (L), width (W), thickness (T), surface area (SA), volume equivalent sphere diameter (VESD), degree of convexity, and many others [25–27]. Since each particle is uniquely numbered, the 3D images and geometrical quantities can be easily cross-correlated.

Due to the fact that extremely fine particles are difficult to accurately resolve using µCT, since the minimum voxel size is around 1 µm, and a particle image needs about 10 voxels across it to obtain an accurate shape characterization [24], all particles of a size smaller than 20 µm were sieved and excluded from the scanning. Since the reference sand only contained particles greater than 20 µm size, for Sand #1 to #5, actually all particles that passed the 20 µm sieve were discarded. Therefore, the size range of particles used in the mortar mixes and in the µCT analysis was identical. Further details of this combined µCT and spherical harmonic method can be seen in two recent review articles [22,28].

2.2.2. Mortar testing protocol

The objective behind these experiments was to explore the effect of different kinds of sand particles on the wet packing density and workability of mortars, while only varying sand particle shape, not particle size distribution. There are of course some differences in how different shape sand particles interact with the square sieve openings [29], but these differences were probably small for this range of sand shapes and so were ignored. Therefore, all six sands were size-proportioned according to sieve analysis in the same way, as shown in Table 4, and denoted the W2360 size proportioning. The W600 size proportioning is also defined in Table 4. The mixing procedure was as follows: (i) weighed water (245 g) in mixing bowl; (ii) added 700 g of cement to the water and mixed for 30 s using a mixer with a blade rotating axially in a planetary motion at a speed of 60 rpm; (iii) added 1350 g of the W2360 proportioned (Table 4) sand during the next 30 s, and continued mixing for an additional 4 min. In total, this mixing procedure took 5 min. During preparation, mixing and testing, all mortars were kept at a temperature of 24.0 °C ± 2.0 °C.

Preliminary feasibility experiments showed that 0.35 is the minimum water to cement ratio required to wet the mix being able to handle it. The amounts of cement and water were calculated according to this ratio and to prepare mortar of constant volume of almost 1 L.

After mixing, the bulk density of mortar [43], also referred to as plastic density, was tested by filling a cylinder of known volume V in two approximately equal layers and vibrating each layer for 5 s on a vibrating table, which was sufficient to achieve a smooth top surface. A final finish of the top surface with a strike-off flat plate was then required. By weighing a measure of volume V, before and after filling it and recording the respective masses, M_e and M_f, we may calculate the density according to BS EN 1015-6: $D = (M_f - M_e)/V$.

Table 4
Sand proportions W2360 and W600 (mass %) used in mortar testing and for petrographic analysis in terms of mass percent retained on sieves. The uncertainty in the percentage retained is very small (< 0.01%), since it is based on a precise mass measurement.

	Sand portion	Percentage	Sand portion	Percentage
W2360	Retained on 1.18 mm	27.7	Retained on 150 µm	20.3
	Retained on 600 µm	35.3	Retained on 75 µm	7.7
	Retained on 300 µm	8.7	Retained on 20 µm	0.3
W600	Retained on 1.18 mm	–	Retained on 150 µm	54.90
	Retained on 600 µm	–	Retained on 75 µm	20.85
	Retained on 300 µm	23.55	Retained on 20 µm	0.70

Several water additions were performed on each mortar mix and each addition was followed immediately by 1 min of mixing followed by another density measurement. The maximum density achieved at a specific optimum water-to-cement ratio (w/c) defines the wet packing density for the subject mortar mix. This water to cement ratio is reached when sufficient water is available for a required volume of paste to hold the sand particles in optimal positions and best fill the voids between the particles, which is defined as the closest state to the saturation point of the mortar system [30,31].

The flow of the hydraulic cement mortar was tested according to the procedure described in ASTM C1437 using a flow mold. The flow table was not used, trying to rely on the particle shape in determining the flow of mortar and eliminating any external factor that might affect it. With every measure, the mold was filled with mortar, lifted and the diameter of the spread was recorded as it slumped down from its original height defined by the mold. Cubic specimens, of edge length 40 mm, were then cast, demoulded after 24 h, and cured in water at (20,0 ± 1,0) °C until 28 days and tested for compressive strength.

2.2.3. Experimental uncertainties

The main experimental uncertainties related to the scanning and computing of particle geometrical factors and mass measurements. Many trials were performed for the other measurements to check the repeatability of these processes. Uncertainty estimates were found to be around 0.33% for plastic density, around 0.005% for volumetric water-to-cement ratio, and around 0.5% for slump-flow measurement. Wherever possible, these uncertainties are shown on the figures, except when they were smaller than the size of the data point symbols.

The shape factors used in this paper are based on L, W, and T and their ratios. The primary source of uncertainty in dimensions is the thresholding process. In the X-ray CT image reconstruction process, a voxel can be created at the edge of an object that overlaps the particle and the surrounding epoxy, thus giving it a gray scale between what is typical of a sand particle and that of the epoxy. Therefore, when thresholding, there can be a half voxel length error on either side of a particle, so that the overall dimension is uncertain to within ± 1 voxel. Depending on the size of the voxel, which was determined in the X-ray CT scanning process, this corresponds to an uncertainty in physical length units. Table 5 shows what voxel size was used for scanning each material in each size class, listed in the third column. The variation in this value reflected the variation in the sample diameters and sample straightness, which determined what the voxel size had to be to be able to scan the whole sample diameter over some height range. The fourth column lists the calculated middle point of the size range considered. Note that the value of 2000 μm used for the top size class is only an estimate, since the largest size considered was not measured. The fifth column of Table 5 shows this physical length uncertainty expressed as a percentage of the middle point of a given size range. This value gives an average estimate for particles in that size range. Note that for the same X-ray CT voxel size, a larger particle will have less uncertainty than a smaller particle (e.g., compare the rows 300–600 and 600–1180 rows for Sand 1). The ratios of L, W, and T are estimated to have about twice that uncertainty, in percentage, since the ratio of L/T, for example, should have an uncertainty roughly equal to the uncertainty in L plus the uncertainty in T.

Table 5
Dimensional uncertainties based on ± 1 voxel length. The dimensional uncertainty is 1 voxel times the voxel size, and the relative dimensional uncertainty is the dimensional uncertainty expressed as a percentage of the middle of the size range considered.

Material	Size range (μm)	X-ray CT voxel size (μm)	Mid-size range (μm)	Relative dimensional uncertainty (% of midpoint of size range)
Standard sand	20–75	1.0184	47.5	2.1
	75–150	1.4532	112.5	1.3
	150–300	6.84819	225	3.0
	300–600	7.53040	450	1.7
	600–1180	6.84819	890	0.8
	1180 +	9.7386	2000*	0.5
Sand 1	20–75	1.0936	47.5	2.3
	75–150	1.9292	112.5	1.7
	150–300	5.47651	225	2.4
	300–600	6.16056	450	1.4
	600–1180	6.16056	890	0.7
	1180 +	9.7647	2000*	0.5
Sand 2	20–75	1.347	47.5	2.8
	75–150	5.13339	112.5	4.6
	150–300	5.81903	225	2.6
	300–600	5.81903	450	1.3
	600–1180	10.26673	890	1.2
	1180 +	19.85940	2000*	1.0
Sand 3	20–75	1.347	47.5	2.8
	75–150	4.10671	112.5	3.6
	150–300	5.81903	225	2.6
	300–600	5.81903	450	1.3
	600–1180	9.92960	890	1.1
	1180 +	19.8594	2000*	1.0
Sand 4	20–75	1.347	47.5	2.8
	75–150	4.10671	112.5	3.6
	150–300	5.81903	225	2.6
	300–600	5.81903	450	1.3
	600–1180	9.9296	890	1.1
	1180 +	19.8594	2000*	1.0
Sand 5	20–75	1.347	47.5	2.8
	75–150	4.79154	112.5	4.3
	150–300	5.13339	225	2.3
	300–600	6.16056	450	1.4
	600–1180	9.9296	890	1.1
	1180 +	19.8594	2000*	1.0

* Estimate, since upper size range of sand retained on 1.18 mm sieve was not measured.

3. Results and discussion

3.1. General petrographic description

Visual testing was undertaken by stereo microscope macro examination of the loose sand grains. The size scale for each image in Fig. 3 is given by the approximate horizontal size of the image in mm. Petrographic thin sections for the six sand types, unwashed as received, were also produced (not shown here). An additional thin section was prepared for a pre-screened, washed, and proportionally mixed W600 sample of Sand 1.

A qualitative analysis of the petrographic thin sections was made and the results summarized in Table 6. The lithology of the sand grains, obtained from QXRD, is also listed in Table 6. Sphericity is a qualitative measure of roundness vs. flatness, angularity is an estimate of the surface texture, grading assesses the width of the particle size distribution, and cleanliness is a measure of how much very fine particles are clinging to the larger sand grains. All four visual and subjective assessments run from 1 to 5. The scales based on the judgement of the petrographer are: Sphericity (1 = rounded to 5 = elongated and flaky), Angularity (1 = smooth surface texture to 5 = rough uneven texture), Cleanliness (1 = clean with no retained material to 5 = extremely dirty and many small particles attached), and Grading (1 = wide particle size spread to 5 = monosize or at best bimodal distribution).

Despite the valuable subjective results listed in Table 6, which do draw distinctions between different particle types, the descriptive petrographic shape specifics, specifically sphericity, angularity and grading, for the different sand particles will show in the course of this paper to be insufficient to predict the plastic performance of different types of sand in fresh mortars and their suitability for a particular

Fig. 3. Photos from macro examination of unsieved Standard CEN sand, Sand 1, Sand 2, Sand 3, Sand 4, Sand 5, and Sand 1-W600. The width of each image is given in order to approximately define the image scale.

Table 6
Petrographic and lithology description (Sp = Sphericity, An = Angularity, Cl = Cleanliness, Gr = Grading).

	Shape description	Lithology	Sp	An	Cl	Gr
Standard sand	Sub-rounded clean equant sand	Mainly quartz with lesser feldspar, volcanics, metaquartzite and siltstone	2	2	1	2
Sand 1	crushed highly angular shards and elongate rock fragments	Limestone (biomicrite) with less biosparite, calcite spar	4	3–4	5	5
Sand 2	crushed highly angular shards and elongate rock fragments	Limestone (biomicrite) with less biosparite, calcite spar	3	4	5	4
Sand 3	crushed angular shards and elongate rock fragments	Limestone (Oosparite and pelsparite) with less biosparite/micrite and calcite spar	3	4	3–4	4
Sand 4	Sub-angular crushed rock with some shards and elongate fragments	Metamorphosed basic and ultrabasic igneous rocks	3	3	3	4
Sand 5	Well-rounded to sub angular sand.	Highly-rounded limestone, quartz and feldspar	1–2	2	1	1
Sand 1 –W600	Crushed limestone highly angular shards and elongate rock fragments	Limestone (biomicrite) with less biosparite, calcite spar	4	4	1	2

application. This means that these descriptive petrographic measures insufficiently characterize the shape properties of the particles that are relevant for rheological performance.

3.2. Physical properties

All six types of sand were analysed. Unwashed and as-received sand samples were tested for relative density and for absorption according to ASTM C128 [32]. W2360 proportioned samples were tested for density using a gas pycnometer. All samples were dried in an oven to constant mass before testing. The results obtained are shown in Table 7.

Assuming that the unwashed and W2360 sands had the same relative density, being from the same material, good agreement existed between the ASTM C128 method and the method of gas displacement, with the highest differences recorded in the case of Sand 4 and Sand 5, 1.8% and 1.1%, respectively. These slight differences might have been due to the precision of these tests or to the higher porosity and partly closed pores for Sand 5, which would affect the nitrogen BET results and was later confirmed by fluorescence microscopy. For Sand 4 and Sand 5, with their higher water absorption, any misjudgment of the fine particles saturated surface-dry condition required for testing the specific gravity, might lead to increased error while taking the measures because of the trapped water inside the pores. Having said that, the He-pycnometer results make sense based on the known density values of the minerals that make up the sands (see Table 6) [33,34].

Table 7
Density and absorption of sand samples (SG = specific gravity).

Unwashed, as received	Apparent SG	Absorption, %	W2360	Density (He-pycnometer), kg/m^3
Standard sand	2.64	1.6	Standard sand	2.64
Sand 1	2.70	1.6	Sand 1	2.71
Sand 2	2.71	1.0	Sand 2	2.72
Sand 3	2.71	0.9	Sand 3	2.71
Sand 4	2.76	3.2	Sand 4	2.71
Sand 5	2.71	2.4	Sand 5	2.68

3.3. Population and minimum sample size for μCT scanning

The result of μCT scanning and spherical harmonic analysis was large numbers of analysed particles for each sand type and particle size class. The following geometrical parameters were computed, based on the spherical harmonic expansion, for each sand particle:

- Particle volume, V (μm^3)
- Particle surface area, SA (μm^2)
- Surface area divided by surface area of sphere with same volume as particle, SA/SASD
- Diameter of sphere with same volume as particle (volume equivalent sphere), ESD (μm)
- Trace of moment of inertia tensor divided by trace of moment inertia tensor for volume-equivalent sphere, I ratio
- Length (L), width (W), thickness (T) (μm), L/T and W/T
- Convexity, ratio of particle volume to the volume of its convex hull. Other shape parameters were also computed and further use of them will be made in a subsequent paper.

The length L is defined as the largest surface-surface distance in the particle. W is defined similarly, except that it must be perpendicular to L, and T is again defined similarly, except that it must be perpendicular to both L and W. Since they are mutually perpendicular, the dimensions L, W, and T define a minimum dimension rectangular box into which the particle just fits. There are two independent ratios of these quantities, L/T, and W/T, which serve as approximate “aspect ratios” of the particle. Handling this amount of data for all the particles and all the shape parameters required statistical calculations and assessment of values like the mean, the median, and the standard deviation (width of distribution).

An open question is how many particles are required to be measured so that accurate values of various averages and distributions of geometrical parameters can be achieved [29]. This cannot be determined a priori. However, statistical quantities for the main parameters were computed on samples of decreasing size randomly selected from the main population. The smallest number of particles that still gave the same statistical results was taken to be a lower bound on the number of particles needed for accurate results. This result can be used in the future to reduce the number of scanned particles needed and therefore the time and effort needed for similar studies.

A first exercise was to study the particles retained on the 150 μm sieve and passing the 300 μm sieve for the CEN sand. Computationally, a particle was retained on this sieve if its value of W was such that 150 μm < W < 300 μm. The value of W is regarded as being closely related to sieve opening size, though there can be particle shape-related issues that affect how close this relationship actually is [29,35,36]. Statistical analysis was performed on all the scanned particles in this size class, a total of 5049 particles, as well as on samples of smaller sizes containing only 1000, 500 and 100 particles that were randomly selected from the total. Related statistical quantities are shown in Table 8, where we observed good agreement for all the parameters as a function of sample size, especially L/T and W/T, within the uncertainties listed in Table 5. This would indicate that about 500 particles was a lower bound for the number of particles necessary to give accurate statistical results and down to 100 particles for certain shape parameters. Previous work on crushed waste glass particles, which were probably more non-spherical than these sand grains, indicated that less than 100 particles would give valid statistical results for many shape parameters, including the aspect ratios L/T and W/T [29]. Note that in Table 8, the first quartile Q1 for a shape parameter means that 25% of the particles have a shape parameter value less than Q1.

Even the particle volume and surface area, which were of order 6 or 7 digits, agreed well when looking at the magnitude of the standard deviations down to a sample size of 500 particles. The same exercise was repeated on all the particle size ranges for all six sand types and found similar results.

Table 8
Statistical computations for different sample sizes of Standard CEN sand (150–300 μm). SE Mean: standard error of the mean; Q1: first quartile; Q3: third quartile [37].

Variable	N	Mean	SE Mean	St. Dev.	Minimum	Q1	Median	Q3	Maximum
V (μm^3)	5049	2717424	34892	2479265	334438	1245972	1754676	2990204	17856526
V (μm^3)	1000	2806607	80625	2549572	426865	1274085	1772853	3114583	13811549
V (μm^3)	500	2814386	112176	2508335	426865	1268132	1837169	3243261	12959641
V (μm^3)	100	3304716	294416	2944162	674581	1418402	1952334	4294383	12959641
SA (μm^2)	5049	106722	813	57779	27900	68976	85967	122187	415380
SA (μm^2)	1000	109212	1898	60035	33858	69777	87614	126132	349893
SA (μm^2)	500	109598	2676	59826	33858	69307	89130	127991	339254
SA (μm^2)	100	122370	6869	68685	47566	74149	94346	155537	302620
SA/SASV	5049	1.2265	0.00105	0.0745	1.062	1.1735	1.215	1.268	1.705
SA/SASV	1000	1.2271	0.00221	0.07	1.062	1.1772	1.218	1.266	1.49
SA/SASV	500	1.2262	0.00317	0.0708	1.087	1.177	1.216	1.2637	1.49
SA/SASV	100	1.2385	0.00789	0.0789	1.088	1.1812	1.232	1.2833	1.49
ESD (μm)	5049	162.02	0.589	41.84	86.12	133.51	149.65	178.75	324.29
ESD (μm)	1000	163.56	1.35	42.77	93.42	134.5	150.16	181.19	297.68
ESD (μm)	500	163.89	1.91	42.62	93.42	134.29	151.96	183.65	291.43
ESD (μm)	100	172	4.7	47.02	108.81	139.4	155.07	201.63	291.43
I ratio	5049	1.2912	0.00253	0.1795	1.038	1.168	1.249	1.359	2.897
I ratio	1000	1.2906	0.00532	0.1682	1.055	1.1705	1.248	1.3588	2.164
I ratio	500	1.2895	0.00764	0.1708	1.059	1.169	1.2455	1.361	2.016
I ratio	100	1.3184	0.0179	0.1795	1.059	1.1795	1.2795	1.4175	1.833
L/T	5049	1.9555	0.00731	0.5191	1.1016	1.5898	1.8477	2.1963	5.8407
L/T	1000	1.9557	0.0161	0.5083	1.1016	1.6026	1.8587	2.1754	4.74
L/T	500	1.9454	0.0227	0.5084	1.1047	1.5971	1.8363	2.1835	3.9731
L/T	100	2.0258	0.0556	0.5564	1.1251	1.6327	1.9344	2.4278	3.7427
W/T	5049	1.4959	0.0049	0.3485	0.9466	1.2424	1.4188	1.6649	3.4268
W/T	1000	1.4994	0.0112	0.3551	0.9466	1.2433	1.431	1.6661	3.3937
W/T	500	1.4736	0.0158	0.3535	0.9466	1.2131	1.4056	1.6442	3.3937
W/T	100	1.5301	0.0408	0.4085	0.9466	1.2169	1.4517	1.6854	3.3937

Table 9
Statistical parameters for different sample sizes (N) for Sand 4.

Sample	N	Mean	St. Dev.	SE Mean	t-value	p-value	Confidence limits
V – all	13274	2099175	2040749	17713	–	–	–
V – 5000	5000	2103318	2019536	28561	−0.12	0.902	−70021, 61735
V – 1000	1000	2151015	2112073	66790	−0.75	0.453	−187415, 83733
V – 500	500	2025506	2006431	89730	0.81	0.421	−105998, 253335
V – 100	100	1964047	2170485	217048	0.62	0.536	−296922, 567177

The *t*-test for unequal sample sizes was used to assess the statistical significance of the average values found [37]. This study was performed on Sand 4, where the total population consisted of 13 274 particles and the particle volume was taken as the example measure in the following. The average value of particle volume from the main population was compared to the average values from samples of reduced sizes consisting of 5000, 1000, 500 and 100 particles. Particle volumes were respectively referred to as V-all, V-5000, V-1000, V-500 and V-100. We tested the null hypothesis that there was no statistical difference between the mean values at a significance level 0.05 and 95% confidence interval when the size of the sample was reduced. When the p-value from the *t*-test is less than the significance level, the null hypothesis should be rejected. Statistical parameters were shown in Table 9.

In all confidence limits in Table 9, it was noticeable that one bound was a negative number and the other bound was a positive number. So the interval encompassed zero. Therefore, the hypothesis that there is no difference between the whole population and smaller samples is supported by the data. From the t-values, corresponding p-values were calculated and found to be greater than the significance level 0.05. We were not able to claim the differences to be statistically significant and we failed to reject the null hypothesis; the mean values from the whole population and smaller samples were not statistically different. This finding is observed in Fig. 4, which illustrates the spread of data related to particle volume for the whole population and different smaller sample sizes. The dashed lines connecting the means and the medians are all quite vertical, showing a similar central tendency for all five distributions irrespective of the sample sizes taken. Some of the smaller sample sizes do not include the large outliers in the full data set, but that does not significantly change the statistics. Therefore, reducing the number of particles during μCT scanning would be possible without affecting the statistical interpretation of collected data.

3.4. Particle shape analysis

Geometrical particle shape analysis, using the parameters listed above (Section 3.3), was applied to all size ranges from all six different sand types. After gathering and classifying statistical data related to particle shape parameters, L/T and W/T, 2D shape histograms were prepared trying to classify the different particles in each size range following their prolate or oblate character, following a previous study [38]. Parameters defined below will serve to help summarize this large mass of data into usable forms.

The numbers listed in the cells of Table 10 are the numbers of particles falling in each separate range of L/T and W/T. For example, the number of particles having L/T between 2.5 and 3.0 and W/T between 1.0 and 1.5 is 673, and so belong to the class (2.5–3.0, 1.0–1.5). Any cells that have W/T > L/T are of course empty of particles, since by definition L ≥ W ≥ T, so that L/T ≥ W/T.

Some valuable insights can be drawn from Table 10 about particle shape. The spherical tendency (Sph-t) of a particle class is defined as the ratio of the number of particles in class (1.0–1.5, 1.0–1.5) divided by the total number of particles, expressed as a percentage. Since the particles in this cell are more equi-axed, this parameter serves as a measure of how many particles were closer to being spheres out of the total. In Table 10, Sph-t was equal to 10.4% and indicates particles with L, W and T closer to being equal. The particles on the diagonal line, having L and W of similar scale and both larger than T, are considered to have an oblate character. The sum of the number of particles on the diagonal of Table 8, divided by the total number of particles, is defined as the oblate tendency (Ob-t). The value of Ob-t was 21.9% using the data in Table 10. If one examines the bottommost filled row, neglecting the first bin, which was associated with more equi-axed particles, the other bottommost-row particles tend to have L much larger than both W

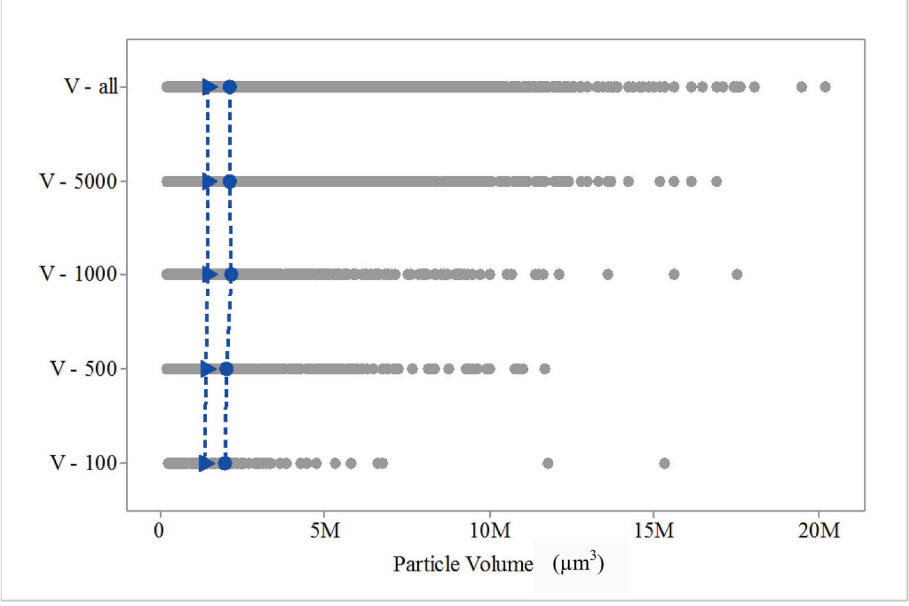

Fig. 4. Individual Value Plot of V - all, V - 5000, V - 1000, V - 500, V – 100 (M = million; ► median; ● mean).

Table 10
L/T and W/T shape aspect histograms of particles from Sand 3 (75 μm–150 μm), 27 130 total particles.

W/T \ L/T	1 - 1.5	1.5 - 2.0	2.0 - 2.5	2.5 - 3.0	3.0 - 3.5	3.5 - 4.0	4.0 - 4.5	4.5 - 5.0	>5.0	>6.0
>5.0	0	0	0	0	0	0	0	0	0	0
4.5 - 5.0	0	0	0	0	0	0	0	0	0	0
4.0 - 4.5	0	0	0	0	0	0	1	0	0	0
3.5 - 4.0	0	0	0	0	0	7	11	4	0	0
3.0 - 3.5	0	0	0	0	54	86	35	10	6	1
2.5 - 3.0	0	0	0	199	361	250	145	35	22	2
2.0 - 2.5	0	0	638	1255	794	366	147	55	23	4
1.5 - 2.0	0	2216	3905	1762	707	220	92	32	9	0
1 - 1.5	2818	7267	2680	673	179	43	11	3	2	0

and T, showing a prolate tendency. The sum of these bins in this row, divided by the total number of particles, is defined as the prolate tendency (Pr-t). In Table 10, the value of Pr-t was 40.0%.

An additional shape factor, another more general measure of oblate tendency, is called OP-F and defined as the ratio of Ob-t to Pr-t:

$$\text{OP-F} = \text{Ob-t} / \text{Pr-t}$$

The larger the value of OP-F, the more the scanned particles tended towards a more oblate shape, with a value of unity for equi-axed particles. A value less than one indicates a more prolate character. This parameter will be used to summarize particle shape into either more or less prolate (less or more oblate) categories.

We present two videos to simulate the difference in shape between two different sand particles retained on a 20 μm sieve:

Supplementary video related to this article can be found at https://doi.org/10.1016/j.cemconcomp.2018.12.018.

As the amount of analysed data was too large to show in this paper, summarized results of the shape tendency factors for the different types and sizes of sand particles are shown in Table 11. Table 11 classifies the sand particles based on their tendency towards an oblate character or a prolate character, comparing them always to the standard sand, using the OP-F parameter. Each section of Table 11 is for a different sand size range, and the sands are ordered from left to right by the decreasing value of the OF-F parameter. The CEN sand, for every size range, always has the highest value of OP-F, closest to unity. Sand 5 is always next, and Sand 4 is always lowest, but the order from left to right of the other sands varies between size ranges. Since for every particle size range considered, the CEN standard sand and Sand 4 were always on opposite ends of the prolate spectrum, these two sands were chosen to have further shape analysis, and illustrate what would be found for the other four sands, which would fall in-between these two limiting materials.

In Fig. 5, for the particles retained on the 1.18 mm sieve, the particle surface area was plotted as a function of the ESD diameter, which was defined from the μCT scans and spherical harmonic analysis. The data points were compared to a power trend line representing the theoretical value that would be found for a sphere. The data for the CEN sand was clearly closer to the sphere reference line than was the data for Sand 4.

In Fig. 6, the ratio of surface area from μCT and spherical harmonic reconstruction to the surface area of sphere with the same volume as the particle (SA/SASD) is displayed as a function of ESD. The data points for Sand 4, for any value of ESD, were clearly further away from the sphere value than was the standard CEN sand.

In Fig. 7, the I ratio is plotted as a function of SA/SASD, with both ratios having the unit value only for perfect spheres. The standard sand had almost all particles situated in the bottom left corner while the particles of Sand 4 were dispersed in the opposite corner. This is because the large components of the moment of inertia tensor scale as the square of L/T, so the prolate nature of particles are emphasized using the I ratio.

The results shown in Figs. 5–7 give additional support to the previous shape classification for the different sand particles listed in Table 11. The particles from Sand 4 were the least like spheres, being more prolate (less oblate) compared to the standard sand and the other sand types. The four other types of sand were located in between these two extremes, as judged by the shape parameters considered.

Since Sand 5 was so close, in terms of shape parameters, to the CEN sand, it was not further studied in this paper.

3.5. Effect of particle shape on mortar consistency

All mortar tests were conducted according to the protocols described in Section 2.2.2 using the W2360 sand size distribution. The only difference between mortars would be the particle shape of the sand type used. The influence of sand particle shape on mortar consistency, which is a measure of the fluidity or wetness of fresh mortar as judged by the slump-flow measurement, was investigated during these experiments. For each type of sand or a combination of different fractions of sand particles, the slump-flow of mortar was measured and the corresponding volumetric water to cement ratio (w/c, volume of water divided by the volume of cement) determined as water was added to achieve a certain slump-flow.

As shown in Fig. 8, the standard sand needed a smaller amount of water (lower volumetric water:cement ratio) to exhibit the same degree of workability (slump-flow) in mortar mixtures as the other sands. For a given value of slump-flow, the required volumetric water to cement ratio increased from the lowest value found for CEN sand, to Sand 2 and Sand 3, which were almost identical, and finally to the largest w/c value for Sand 4. Sand 1 was excluded from this experiment due to the fact that its particle shape was classified close to Sand 2 and Sand 3 (Table 11), therefore must perform similarly, and to the lesser amounts available from this sand. This order followed the classification of shape character demonstrated in Table 11, showing that the OP-F parameter decreased in the same way, from nearly equi-axed to more prolate character.

3.6. Shape and wet plastic density analysis

3.6.1. Effect of sand type

These trials aimed to compare the effect of sand type on the fresh mortar plastic or bulk density (see Sec. 2.2.2), explaining the behaviour in terms of sand particle shape. The results are shown in Fig. 9. The abcsissa of Fig. 9 uses the volumetric form of the water:cement ratio, denoted with a lower case w/c. The peak of plastic density reached by each type of sand defines its particular packing density. The tighter packing of rounded standard CEN sand happened at low water content, with the highest plastic density found at w/c = 1.12. For larger w/c values, the plastic density decreased below that of Sand 2, Sand 3 and even Sand 4 because of the quick gain in workability with the addition of water and much higher dispersion of solid particles in the water [39].

Table 11
Shape tendency and factors for different sand particles.

Oblate Character	1.18 mm	CEN	Sand 5	Sand 2	Sand 1	Sand 3	Sand 4	Prolate Character
	Ob-t	42.9%	29.9%	17.2%	14.2%	11.2%	11.2%	
	Pr-t	41.4%	31.8%	23.3%	22.0%	22.4%	29.6%	
	OP-F	1.04	0.94	0.74	0.64	0.50	0.38	
	Sph-t	26.3%	10.4%	7.8%	2.4%	2.4%	1.6%	
Oblate Character	600 µm	CEN	Sand 5	Sand 1	Sand 3	Sand 2	Sand 4	Prolate Character
	Ob-t	45.7%	33.0%	14.0%	15.9%	16.5%	13.8%	
	Pr-t	43.4%	35.5%	16.5%	24.8%	26.6%	30.1%	
	OP-F	1.05	0.93	0.85	0.64	0.62	0.46	
	Sph-t	31.9%	19.6%	2.4%	4.6%	4.6%	4.2%	
Oblate Character	300 µm	CEN	Sand 5	Sand 1	Sand 3	Sand 2	Sand 4	Prolate Character
	Ob-t	43.0%	31.9%	17.0%	16.0%	15.0%	15.1%	
	Pr-t	41.0%	39.7%	26.2%	26.0%	25.9%	30.3%	
	OP-F	1.05	0.80	0.65	0.61	0.58	0.50	
	Sph-t	23.4%	18.0%	4.0%	5.0%	4.1%	4.4%	
Oblate Character	150 µm	CEN	Sand 5	Sand 3	Sand 2	Sand 1	Sand 4	Prolate Character
	Ob-t	31.0%	30.7%	17.6%	12.7%	14.9%	15.8%	
	Pr-t	43.2%	48.5%	32.2%	25.2%	30.1%	34.3%	
	OP-F	0.72	0.63	0.55	0.50	0.49	0.46	
	Sph-t	16.5%	19.4%	6.4%	3.1%	4.7%	5.9%	
Oblate Character	75 µm	CEN	Sand 5	Sand 1	Sand 3	Sand 2	Sand 4	Prolate Character
	Ob-t	38.5%	29.8%	25.3%	21.9%	17.4%	18.8%	
	Pr-t	43.4%	48.9%	38.8%	40.0%	34.9%	38.1%	
	OP-F	0.89	0.61	0.65	0.55	0.50	0.49	
	Sph-t	23.8%	19.1%	11.1%	10.4%	6.8%	7.5%	
Oblate Character	20 µm	CEN	Sand 5	Sand 3	Sand 1	Sand 2	Sand 4	Prolate Character
	Ob-t	26.3%	27.1%	25.6%	24.6%	21.7%	17.9%	
	Pr-t	32.1%	46.7%	43.7%	42.6%	38.2%	36.6%	
	OP-F	0.82	0.58	0.59	0.58	0.57	0.49	
	Sph-t	11.9%	16.8%	14.3%	13.6%	10.9%	6.4%	

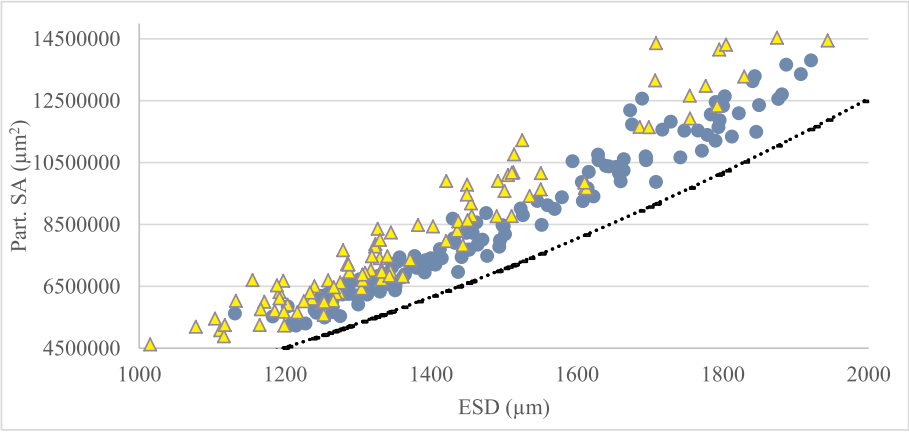

Fig. 5. Scatterplot of particle surface area vs. ESD for particles retained on 1.18 mm sieve (● CEN; ▲Sand 4; … theoretical trend line for perfect spheres).

Data on workability was discussed in Section 3.5.

The more the particles tend to a rounder shape, the more efficiently they are able to be packed at lower volumetric w/c (lower amount of water) [40,41]. This makes any sand similar to Sand 4, with more prolate character, very useful in high water to cement ratios (> 1.90) types of mortar, where it does not lead to rapid gain of fluidity and steep drops in the plastic density of the mix compare to a sand like the CEN standard sand. Sands like Sand 4 are also less vulnerable to bleeding and segregation at high water content, since it had a higher plastic density compared to standard CEN sand.

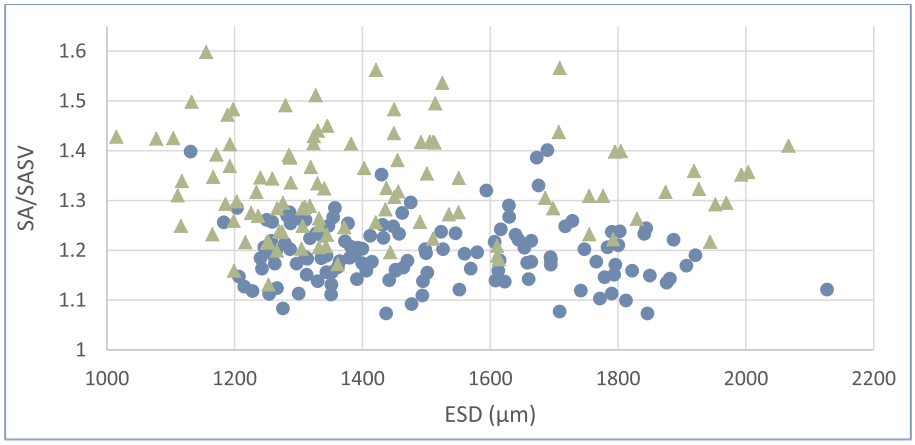

Fig. 6. Scatterplot of SA/SASV vs. ESD for particles retained on 1.18 mm sieve (● CEN; ▲Sand 4).

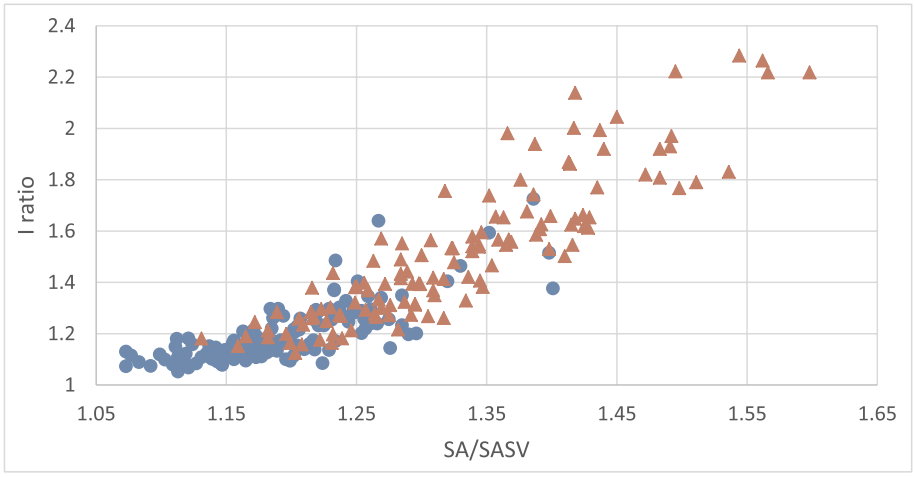

Fig. 7. Scatterplot of I ratio vs. SA/SASV for particles retained on 1.18 mm sieve (● CEN; ▲Sand 4).

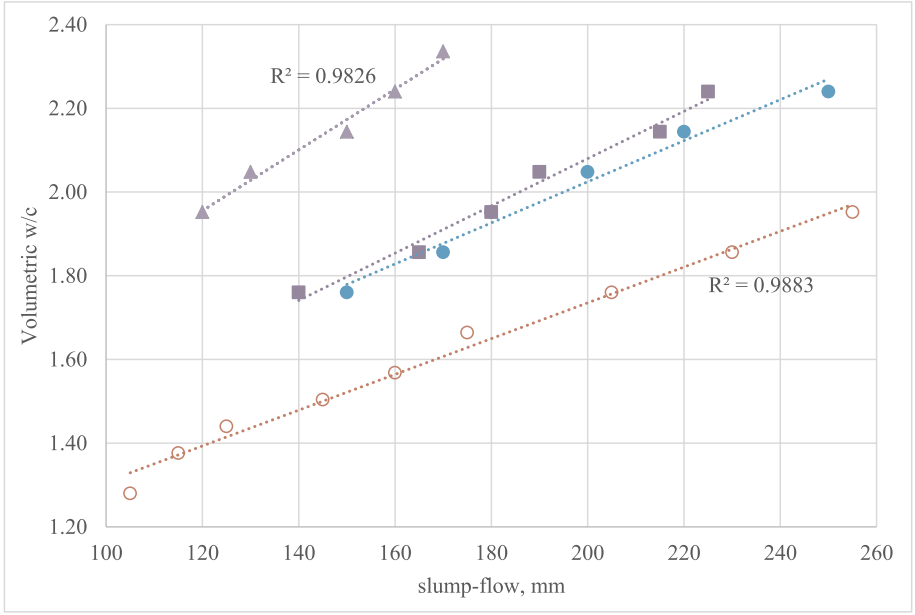

Fig. 8. Representation of volumetric water to cement ratio in relation to mortar consistency (○ CEN; ● Sand 2; ■ Sand 3; ▲ Sand 4).

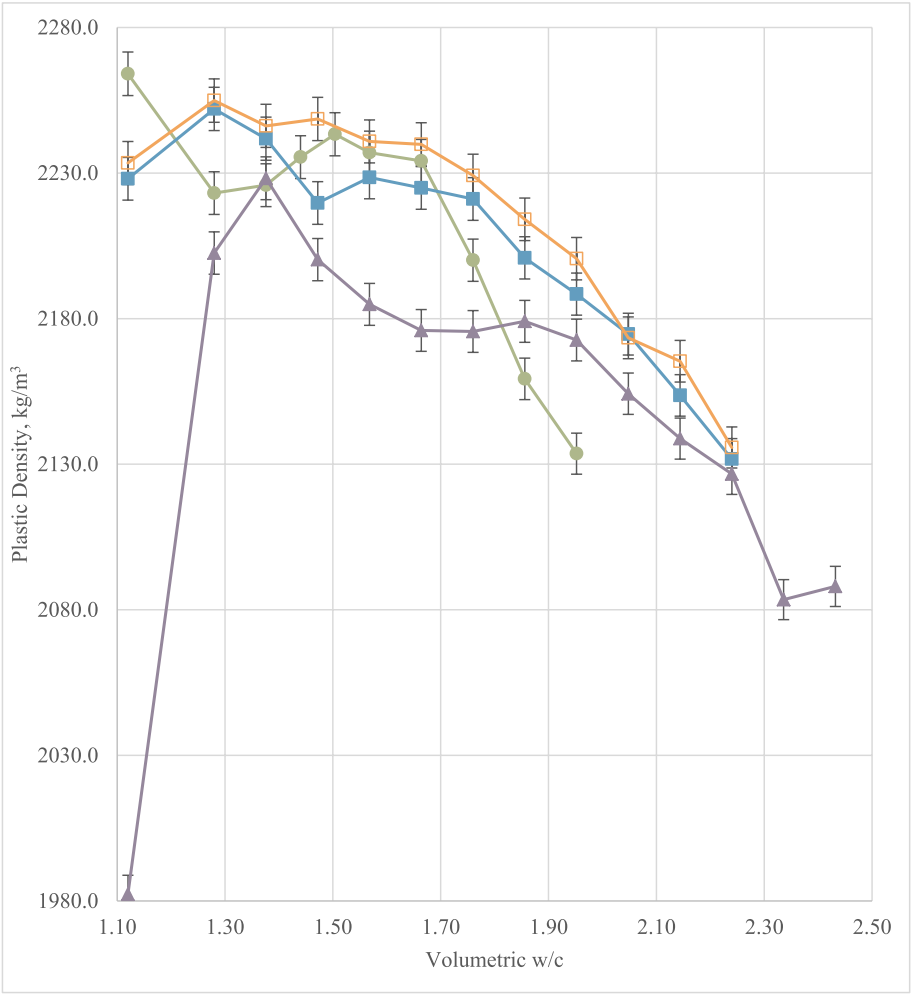

Fig. 9. Representation of mortar plastic density in relation to volumetric water to cement ratio (● CEN; □ Sand 2; ■ Sand 3; ▲Sand 4).

3.6.2. Study on blending various size fractions of different sand types

In this section, the influence of the particle size on the plastic density of mortars made with blended sands was studied. Mortars were prepared by substituting for sand particles of one type, in specified particle size ranges, by particles from the same size range but from different sand types. Plastic (bulk) density was measured with every addition of water. The idea was to see if the particle size range substituted affected how much different particle shapes influenced the plastic density. Such blends could be a remedy in a situation where a sand of inferior quality, where "inferior quality" is defined in terms of the quantities measured in this paper not meeting specifications, is found.

3.6.2.1. Particle size fractions above and below 150 μm. Starting with Sand 4, the most prolate sand, as the base sand, two blended sands were prepared by substituting Sand 2 particles for the size ranges below 150 μm, denoted Sand 4(-150):2, and above 150 μm denoted Sand 2(+150):4. These two types of sand were selected because of their noticeable difference in particle shape.

The plastic density of these two blends vs. volumetric w/c are shown in Fig. 10. Notice the relatively low influence of the particle size range below 150 μm, with the pure Sand 4 and Sand 4(-150):2 data being nearly the same. This could be due to the low mass percentage, 8.0% (see Table 4), that this size range contributes. It also could be due to the fact that the smaller particles tend to occupy the spaces between the larger particles, so that there was sufficient room between the larger Sand 4 particles for either the substituted Sand 2 or original Sand 4 particles. Substituting for the size range above 150 μm added around 48 kg/m^3 to the plastic density at the peak for Sand 4(+150):2, even though the two sand densities were almost the same, due to particle shape. The particle shape of coarser particles with a size above 150 μm is more dominant in determining the packing density of sand particles in mortar mixes than the shape of particles below 150 μm. This could be due simply to their higher contribution by mass (71.7%, see Table 4) in the mix proportions. Or perhaps the coarser particles set the "frame" of the packing, with the smaller particles filling in the gaps between, so that the coarser particles are more influential in achieving a denser packing. Therefore, based on Table 11 and the clear difference in the particle shape, Sand 2 coarse particles with their tendency to a less prolate or more oblate character are able to pack more efficiently showing a considerable addition to plastic density. The influence of finer particles compared to coarser particles on packing density will be studied at the same mass percentage later in this paper.

3.6.2.2. Particle size fractions above and below 300 μm. Blended sands, with Sand 4 again the base sand, were prepared by substituting the particles of size range above 300 μm of Sand 4 with Sand 2 or Sand 3 particles, respectively denoted Sand 2(300):4 and Sand 3(300):4. The plastic density vs. volumetric w/c for mortars using either blended sand are shown in Fig. 11. This substitution with Sand 2 and Sand 3 added around 25 kg/m^3 to the plastic density when compared to the mix containing Sand 4 alone. Particles from Sand 2 and Sand 3, tending to a less prolate and thus more to a equi-axed shape, pack more tightly with less space around the sand grains that must be filled with cement paste.

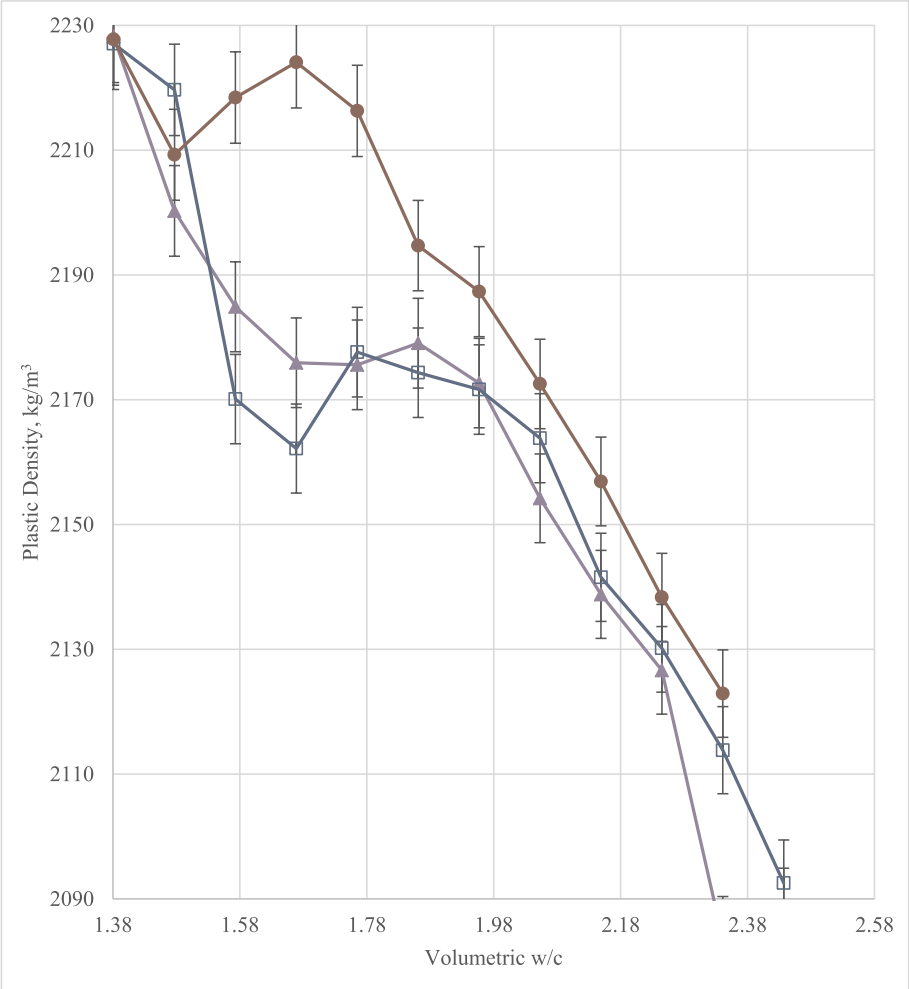

Fig. 10. Representation of mortar plastic density in relation to volumetric water to cement ratio (● Sand 2(+150):4; □ Sand 4(-150):2; ▲Sand 4).

Since Sand 2 and Sand 3 were similar in particle shape, as measured by the parameters used in Table 11, there is not a large difference in plastic densities between the blended sand mortar mixes containing Sand 2 or Sand 3.

3.6.2.3. Influence of the fractions of particles greater than 1.18 mm. The size range of particles greater than 1.18 mm, as measured by sieving, was substituted in Sand 4 by Sand 2, denoted Sand 2(1.18):4. This blend had Sand 2 large particles and the rest Sand 4 particles. Conversely, the size range of particles greater than 1.18 mm, as measured by sieving, was subtituted in Sand 2 by Sand 4, denoted by Sand 4(1.18):2. This blend had Sand 4 large particles, and the rest Sand 2 particles. The results for the plastic density vs. the volumetric w/c are shown in Fig. 12. A difference in plastic density of up to 75 kg/m^3 is found when comparing pure Sand 2 (greater plastic density) and Sand 4 (lower plastic density). Introducing particles from Sand 4 greater than 1.18 mm to Sand 2 tended to decrease the plastic density when compared to pure Sand 2, and introducing Sand 2 particles larger than 1.18 mm to Sand 4 tended to increased the plastic density when compared to pure Sand 4. The increase or decrease of plastic density was limited to around 10 kg/m^3 based on the shape of the particles and related to the proportion in mass of these particles in the mortar mix. Whenever prolate particles as determined by μCT are introduced into a mix, the plastic density decreases, while the introduction of more oblate/less prolate particles, able to pack more efficiently and tightly, increases the plastic density.

The gradual introduction of more oblate/less prolate particles, as determined by the μCT and spherical harmonic determination of the OP-F parameter, into a mortar mix of prolate particles, was studied. The W2360 mix proportions remained the same as listed in Table 4. Sand 4 was the base sand, which had the lowest value of OP-F for each size range. Sand 4 was gradually substituted by Sand 2 particles. The replacement started by the particles of size range greater than 1.18 mm, then included the 600 μm as well. Then the 300 μm was added, and finally the 150 μm range was included. These blends are denoted, respectively, by Sand 2(1.18 mm):4, Sand 2(600):4, Sand 2(300):4, and Sand 2(150):4. Replacement of the smaller particle size ranges was deemed to be unnecessary, judging by the results of Sec. 3.6.2.1. In Fig. 13, the gradual replacement of Sand 4, starting with the size range above 1.18 mm and ending with the size range above 150 μm, with Sand 2, a less prolate particle, was accompanied by a monotonic increase of plastic density of up to 75 kg/m^3. This was caused by a steady increase in packing density with the increased replacement of the more prolate particles (Sand 4) by the more oblate particles (Sand 2). This increase in packing density is directly related to the increase in weight of the fraction of oblate particles in the mortar. The higher the relative mass percentage of less prolate particles replacing Sand 4 particles, the more the mortar plastic density increased.

For the same blended sands, a parallel examination of the slump-flow showed how the required water to attain a certain value of flow decreased with the gradual substitution of Sand 4 with portions from Sand 2, reflecting the higher OP-F value of Sand 2 with respect to Sand

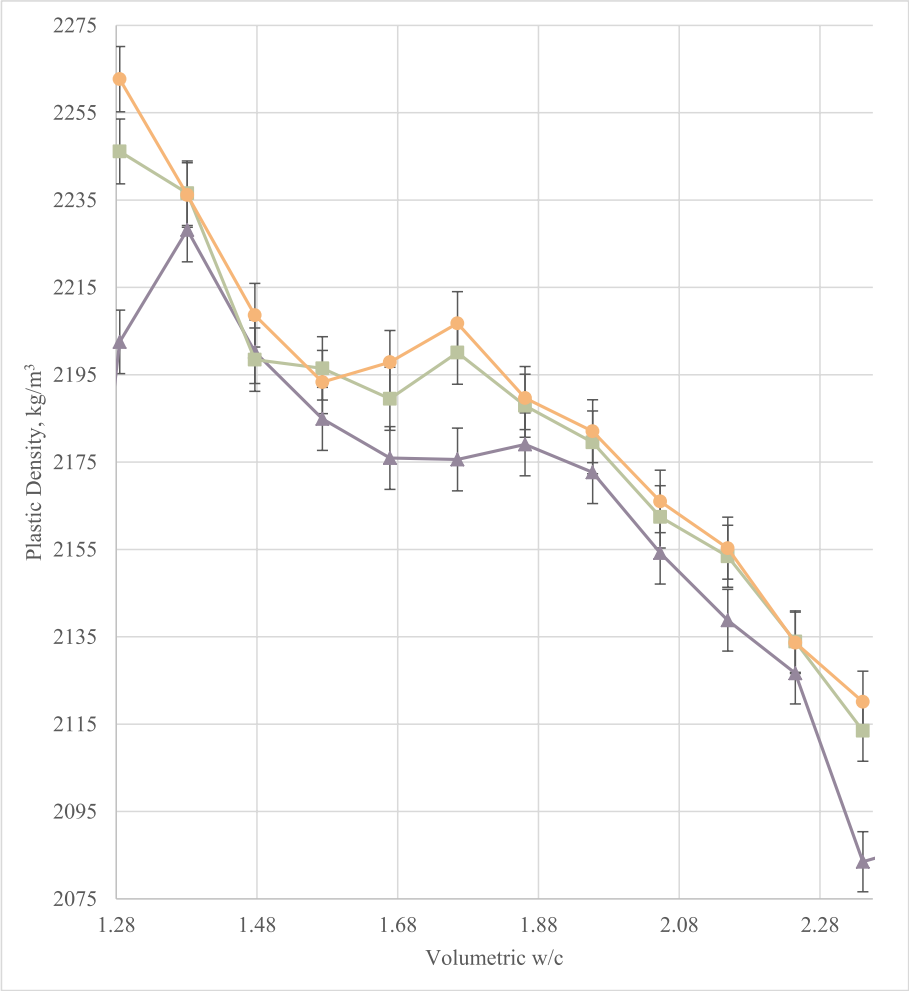

Fig. 11. Representation of mortar plastic density in relation to volumetric water to cement ratio (● Sand 2(300):4; ■ Sand 3(300):4; ▲Sand 4).

4. Results are displayed in Fig. 14. To attain a given slump-flow (consistency level), the water demand increased up to 25% when moving from 100% S to 2–100% Sand 4. Here the μCT/spherical harmonic method is useful as a classification method for sand particles measuring the influence of shape and surface irregularities not only on packing density but also on the consistency or slump-flow of cementitious mixtures.

3.6.2.4. Influence of almost equal fractions of particles of different sizes. After having substituted for various particle size ranges, and examined the relative influence of larger vs. smaller particles, a more specific question can be asked: which particle size range has the most pronounced impact on plastic density, and how does relative mass percentage affect this result? Looking at the mix proportions in Table 4, it was noticeable that the mass fraction of particles retained on the 1.18 mm sieve was equal to the sum of the three mass fractions retained on the 20 μm, 75 μm, and 150 μm sieves. It was therefore interesting to conduct comparative trials starting with Sand 2 or Sand 3, then interchanging the portion above 1.18 mm with Sand 4, denoted Sand 4(1.18):2, and also interchanging the portion below 300 μm with Sand 4, denoted Sand 2(300):4. In these two cases, the mass fraction of interchanged sand was the same, so the effect on plastic density would only be due to particle size and shape. The results are compared in Fig. 15 for plastic density plotted vs. volumetric w/c. In Fig. 15, it can be seen that replacing the fine portion of Sand 2 with Sand 4 particles caused the plastic density to drop by more than 45 kg/m^3. The same was observed when repeating this exercise starting with Sand 3 instead of Sand 2. The fine portion of the particle size distribution plays a major role within the mortar by filling the gaps between coarser particles, leading to higher density. The more prolate Sand 4 particles do not pack as well between the larger Sand 2 particles. Replacing the coarser fraction of Sand 2, with the same mass fraction, has less effect on plastic density than the fine fraction, as can be seen in Fig. 15. When the more prolate Sand 4 particles, in the size range greater than 1.18 mm, were substsituted for Sand 2 particles, the drop in plastic density was only of the order of 10 kg/m^3.

The slump-flow of the same blended-sand mixtures was also measured. In Fig. 16, the greater influence of the portion of particles below 300 μm in controlling the flow at all levels of workability was observed when comparing the mixes with Sand 2 and Sand 2(300):4. When this portion in Sand 2 was replaced with more prolate particles from Sand 4, the amount of water needed for a certain flow increased by almost 10%.

The particles above 1.18 mm had limited influence on the required water for a given workability when interchanging this portion between Sand 2 and Sand 4. However, as seen within the data points encircled in red in Fig. 16 at workability levels above 200 mm flow and when comparing the water demand of Sand 2 and Sand 4(1.18):2, we noticed an increased demand of water for the same workability when introducing the prolate coarser particles in the mix. At such levels of workability, the coarser particles might have increasing influence on rheology, yield stress and viscosity of concrete and the required water might therefore increase in order to actively mobilize them and enable them to move the slump further from the centre when measuring the slump-flow of the mortar mix [42]. These findings can be rechecked

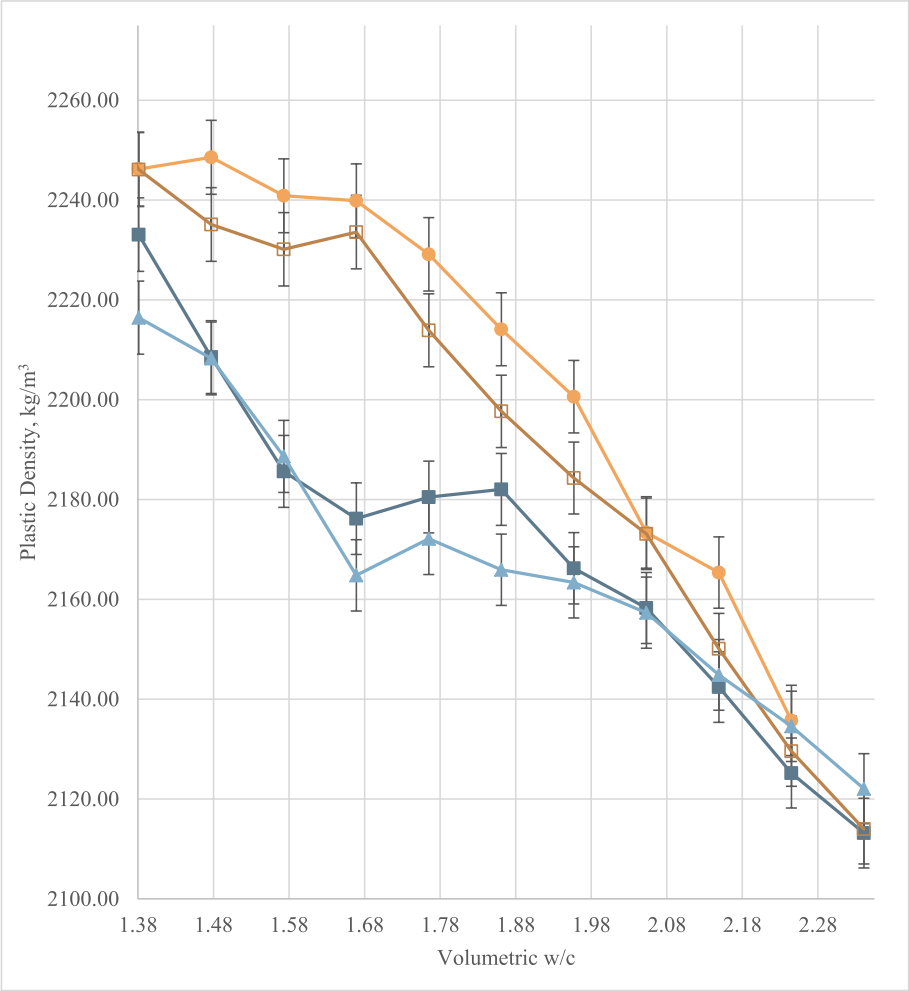

Fig. 12. Representation of mortars plastic density in relation to volumetric water to cement ratio (● Sand 2; ■ Sand 2(1.18):4; □ Sand 4(1.18):2 ▲Sand 4).

and validated with other workability or rheological testing methods or with coarser aggregates as in the case of concrete.

3.6.2.5. Influence of shape on packing density. In this section, we tried to find a relationship between the packing density and shape factors. The shape factor OP-F from the shape histograms in Table 11 in Section 3.4 was found to be the most suitable, i.e. varied the most in an expected way with mortar packing density. This was to be expected, as the various substituted sand studies were undertaken with the relative values of OP-F in mind. Values of OP-F weighted for different combinations of particles of different types and sizes were calculated to reflect the proportion of each sand in the various sand combinations considered above. If a certain combination contained *i* different types and sizes of particles, where *i* runs over both sand type and size fraction, mass percentage p_i, and shape factors OP-F_i, the weighted OP-F would be equal to $\Sigma(p_i*\text{OP-}F_i)$. Packing densities, which were defined as the maximum plastic density over all volumetric w/c considered, were taken from all the previous experiments and graphs for both mixed and pure sands and the collected data were plotted in Fig. 17. The relationship between OP-F and packing density appears to be roughly positive linear. Most of the data points collected on Fig. 17 are falling within or very close to the 95% confidence interval. With R-Sq equal to 74.9%, the weighted OP-F accounts for 75% of the variance in plastic density, which is very important to consider and can be improved. Additional sand types and shapes should be tested in order to cover more OP-F values between 0.65 and 0.90 and to improve the data fit represented in Fig. 17 that may change, especially with the one data point at OP-F 0.97 related to our standard CEN sand necessary to represent but governing the outline of the fitted line.

4. Conclusions

The shape of sand particles from different sources of aggregates was characterized, and the importance of the geometric shape metrics of the size fractions between 20 µm and 2.36 mm on the workability (slump-flow) and wet packing density of mortars was studied. The combined technique of X-ray microcomputed tomography (µCT) and spherical harmonics was used to analyze three-dimensional particle shape. It was found that the number of particles scanned by µCT and analysed by spherical harmonics could be reduced to 500 or even 100 particles without changing significantly the averages of various shape parameters, within experimental uncertainty. This could have positive impact on the time and effort spent on the preparation and scanning of the samples.

From all the data collected by µCT and computed with spherical harmonics, simpler shape factors as Ob-t, Pr-t, OP-F and Sph-t were proposed and computed from the very large number of particles analysed and used to successfully characterize and classify the six different types of sand studied. Relationships between these shape parameters and mortar consistency and wet packing density were then measured. The water demand for a certain required mortar workability increased as sand particles changed from an equi-axed character to a more prolate character. The particles with a more equi-axed character packed more efficiently at low w/c ratios and showed the highest mortar wet packing

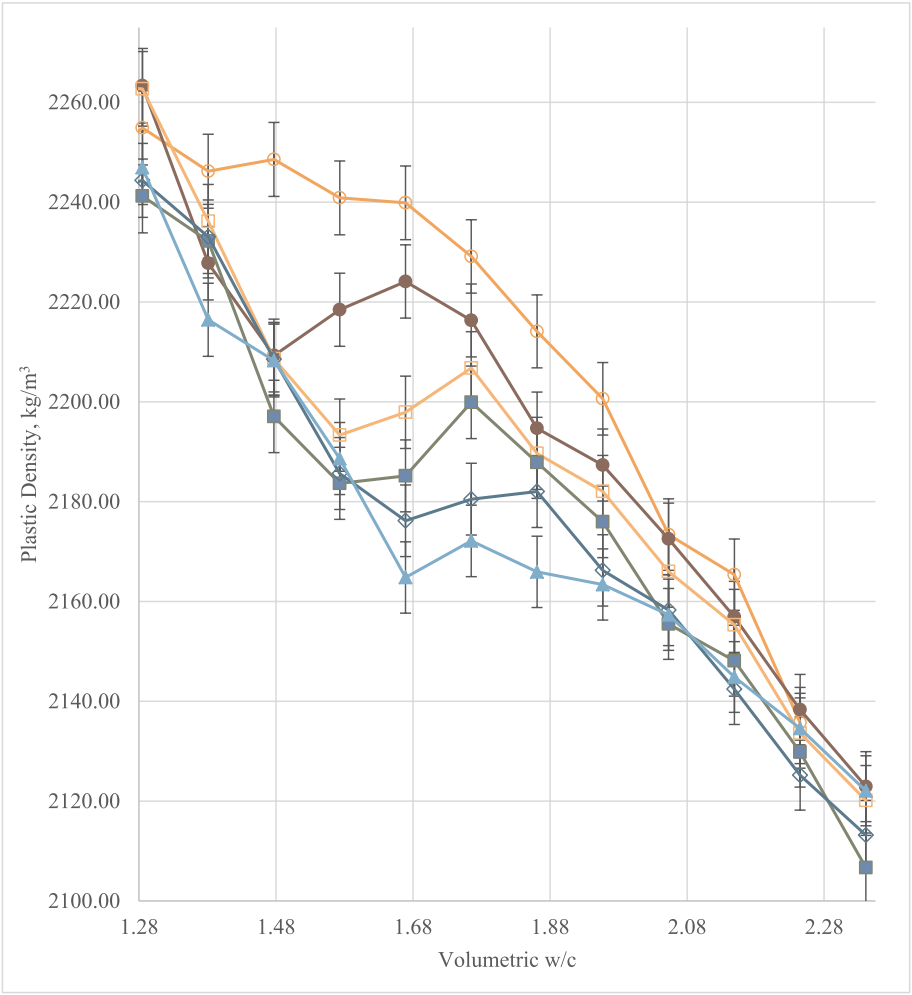

Fig. 13. Representation of mortars plastic density in relation to volumetric water to cement ratio (○ Sand 2; ● Sand 2(150):4; □ Sand 2(300):4; ■ Sand 2(600):4; ◊ Sand 2(1.18):4; ▲Sand 4).

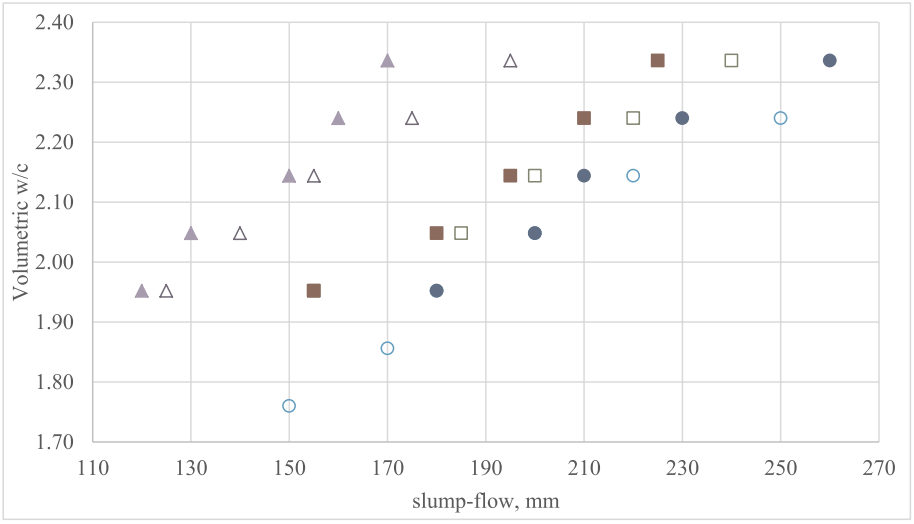

Fig. 14. Representation of volumetric water to cement ratio in relation to mortar consistency in terms of flow (○ Sand 2; ● Sand 2(150):4; □ Sand 2(300):4; ■ Sand 2(600):4; Δ Sand 2(1.18):4; ▲Sand 4).

densities. The magnitude of influence of any particle size fraction was directly related to its mass proportion within the total mix. The higher the mass percent of particles of a specific size, the more this size fraction influenced the wet packing density. But when the comparison was conducted based on nearly the same mass percent, the finer fraction below 300 μm showed greater influence on the values of the wet packing density than the coarser fraction above 1.18 mm in mortars with maximum particle size of 2.36 mm. It was also shown that an approximate linear relationship existed between the shape parameter OP-F and the wet packing density, over all pure and blended sands.

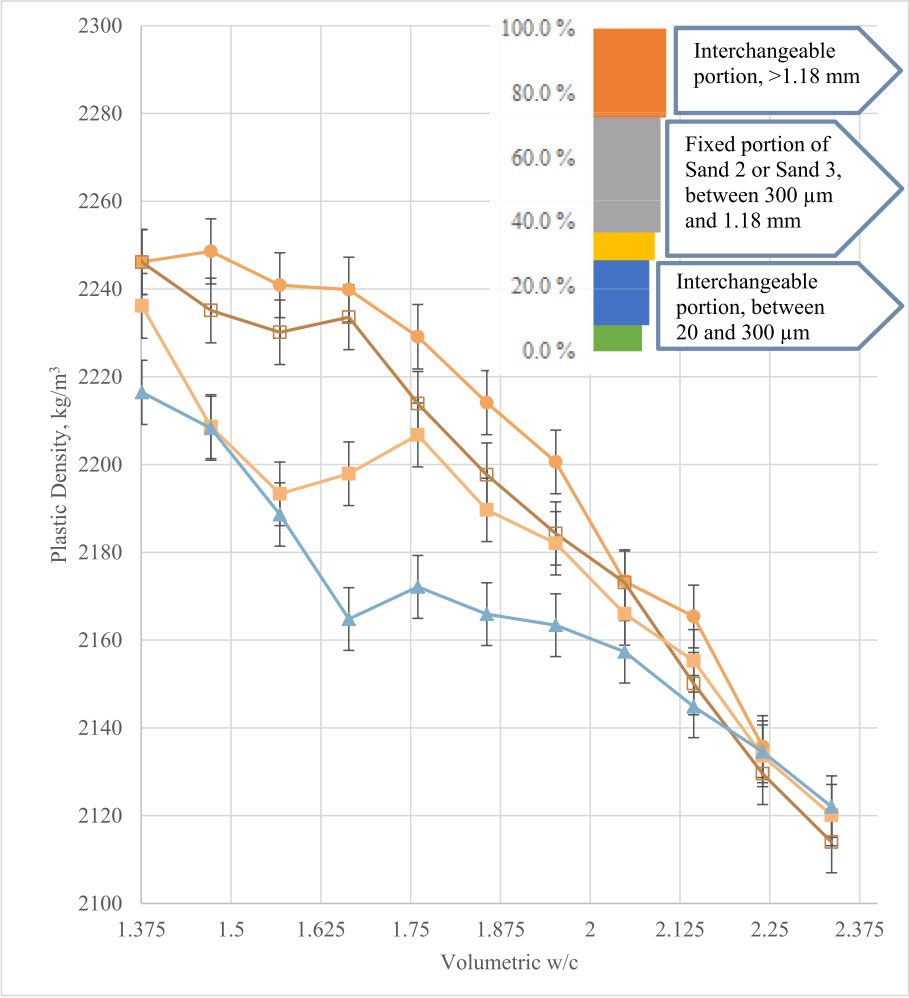

Fig. 15. Mortar plastic density in relation to volumetric water to cement ratio (● Sand 2; □ Sand 4(1.18):2; ■ Sand 2(300):4; ▲Sand 4).

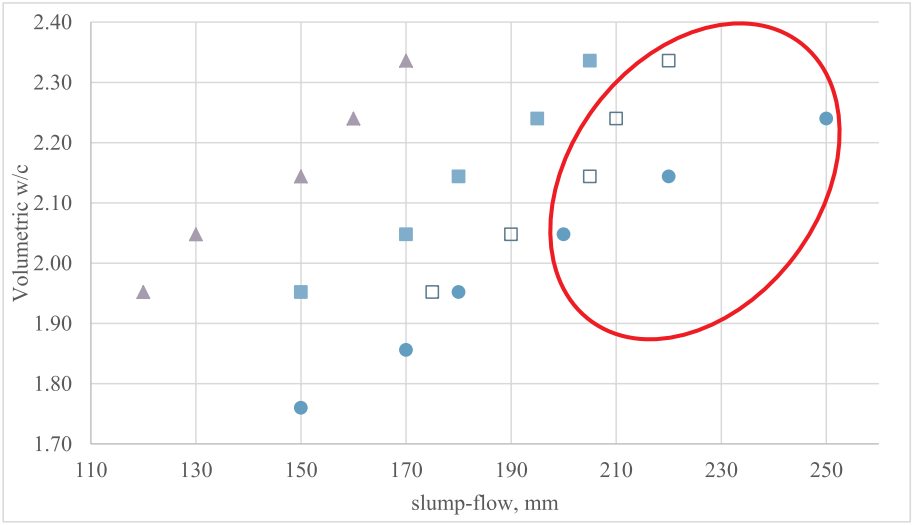

Fig. 16. Representation of volumetric water to cement ratio in relation to mortar consistency (● Sand 2; □ Sand 4(1.18):2; ■ Sand 2(300):4; ▲Sand 4) – the circle in red shows the increased water demand for the same levels of mortar consistency when introducing the prolate coarser particles from Sand 4 into the mix. (For interpretation of the references to colour in this figure legend, the reader is referred to the Web version of this article.)

Additional experiments on different sources of sand, types, and shapes should be conducted to achieve better statistics in this relationship.

As Sand 5 was so close, in terms of shape characterization, to the CEN sand, the two types of sand are expected to perform similarly when mixed in mortars. Therefore the effect of sand 5 (dune sand) as a remedial phase to sand types should be assessed and explored more, whenever inferior performance, due to prolate shaped particles and related to poor mortar initial workability, slump-flow retention or low wet packing density, is faced.

The main experimental uncertainties were adressed and discussed for both the mortar experiments and the particle shape characterization. The experiments described in this paper, along with the data

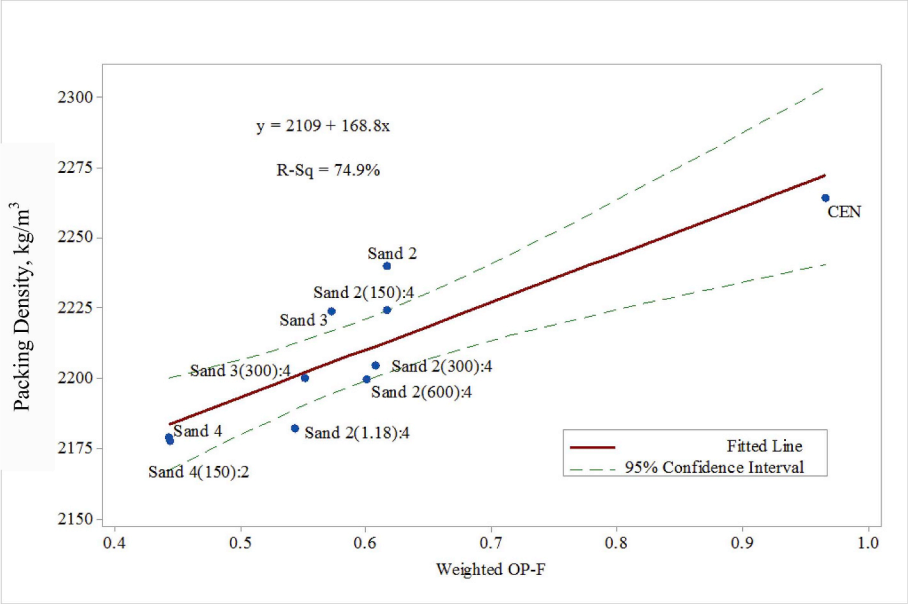

Fig. 17. Relationship between mortar packing density and weighted OP-F, defined for the various pure sand types and mixture of sand types considered in this paper.

generated by X-ray microtomography and spherical harmonics on the particle shape measurement, could serve as a procedure for quality control of crushed sand to evaluate its suitability for different applications.

5. Future work

Some other shape metrics were computed from the X-ray micro-computed tomography and spherical harmonics analysis, including but not limited to convexity, roundness, Corey shape factor, and others. Further use of these parameters will be made in a second paper, which will deal with some other elements that can affect the quality of mortar like the introduction of water reducers in the cementitious mixtures and while working at much lower volumetric water:cement ratios. The possible relation between the shape of fine particles and the compressive strengths of mortar and concrete could be investigated. The aim is to optimize the proportioning of the mortar mixes using locally available sands and so achieve a high performance mortar with local materials. A comparison between actual and μCT measured particle size distributions like the W600 particle size range could be analysed as well.

Appendix A. Supplementary data

Supplementary data to this article can be found online at https://doi.org/10.1016/j.cemconcomp.2018.12.018.

References

[1] Pranay Gupte, Dubai: The Making of a Megapolis, Publisher: Penguin, 2011.
[2] K. Al-Kodmany, M.M. Ali, The Future of the City: Tall Buildings and Urban Design, Publisher: WIT Press, 2013.
[3] O.H. Wallevik, J.E. Wallevik, Rheology as a tool in concrete science: The use of rheographs and workability boxes, Cement Concr. Res. 41 (2011) 1279–1288.
[4] M. Geiker, M. Brandl, L. Thrane, L. Nielsen, On the Effect of Coarse Aggregate Fraction and Shape on the Rheological Properties of Self-Compacting Concrete, Cem. Concr. Aggregates 0149-6123, 24 (1) (2002) 3–6 https://doi.org/10.1520/CCA10484J.
[5] E.P. Koehler, D. Fowler, Research report ICAR 108-2F: Aggregates in self-consolidating concrete, Austin, (2007).
[6] R. Poulin, R.C. Pakalnis, K. Sinding, Aggregate resources: Production and environmental constraints, Environ. Geol. 23 (1994) 221–227.
[7] P. Estephane, K.-A. Rieder, Practical technical solution for clay-contaminated sands used in concrete, MATEC Web Conf. 120 02012, 2017, https://doi.org/10.1051/matecconf/201712002012.
[8] P. Estephane, K.-A. Rieder, Advanced analysis of an engineered solution for high permissible limits of clay in contaminated sands used in concrete, Proceedings of the 1st International ICT Conference on Cement and Concrete Technology, Whittles Publishing, Oman, 2017.
[9] C.F. Ferraris, K.H. Obla, R. Hill, The influence of mineral admixtures on the rheology of cement paste and concrete, Cement Concr. Res. 31 (2) (2001) 245–255 https://doi.org/10.1016/S0008-8846(00)00454-3.
[10] Rolands Cepuritis, B.J. Wigum, E.J. Garboczi, Ernst Mørtsell, Stefan Jacobsen, Filler from crushed aggregate for concrete: Pore structure, specific surface, particle shape and size distribution, Cement Concr. Compos. 54 (2014) 2–16 https://doi.org/10.1016/j.cemconcomp.2014.03.010.
[11] R. Cepuritis, E.J. Garboczi, C.F. Ferraris, S. Jacobsen, B.E. Sørensen, Measurement of particle size distribution and specific surface area for crushed concrete aggregate fines, Adv. Powder Technol. 28 (2017) 706–720.
[12] R. Cepuritis, E.J. Garboczi, S. Jacobsen, Three-dimensional shape analysis of concrete aggregate fines produced by VSI crushing, Powder Technol. 308 (2017) 410–421.
[13] R. Cepuritis, E.J. Garboczi, S. Jacobsen, K.A. Snyder, Comparison of 2-D and 3-D shape analysis of concrete aggregate fines from VSI crushing, Powder Technol. 309 (2017) 110–125.
[14] BS EN 196-1, Methods of testing cement - Part 1: Determination of strength, (2016).
[15] P.M. Chaikin, Aleksandar Donev, Weining Man, Frank H. Stillinger, Salvatore Torquato, Some Observations on the Random Packing of Hard Ellipsoids, Ind. Eng. Chem. Res. 45 (2006) 6960–6965.
[16] F. de Larrard, Concrete Mixture Proportioning, A Scientific Approach, 1999.
[17] G.T. Nolan, P.E. Kavanagh, Random packing of nonspherical particles, Powder Technol. 84 (1995) 199–205.
[18] Jian Zhao, Shuixiang Li, Peng Lu, Lingyi Meng, Teng Li, Haiping Zhu, Shape influences on the packing density of frustums, Powder Technol. 214 (2011) 500–505.
[19] X. Jia, R.A. Williams, A packing algorithm for particles of arbitrary shapes, Powder Technol. 120 (3) (2001) 175–186.
[20] Jiong Hu, Kejin Wang, Effect of coarse aggregate characteristics on concrete rheology, Constr. Build. Mater. 25 (Issue 3) (2011) 1196–1204.
[21] BS 812-103.1: Testing aggregates — Part 103: Methods for determination of particle size distribution — Section 103.1 Sieve tests.
[22] E.J. Garboczi, J.W. Bullard, 3D analytical mathematical models of random star-shape particles via a combination of X-ray computed microtomography and spherical harmonic analysis, Adv. Powder Technol. 28 (2017) 325–339.
[23] ASTM C136/C136M: Standard Test Method for Sieve Analysis of Fine and Coarse Aggregates.
[24] E.J. Garboczi, Three-dimensional mathematical analysis of particle shape using X-ray tomography and spherical harmonics: application to aggregates used in concrete, Cement Concr. Res. 32 (10) (2002) 1621–1638.
[25] S.T. Erdoğan, P.N. Quiroga, D.W. Fowler, H.A. Saleh, R.A. Livingston, E.J. Garboczi, P.M. Ketcham, J.G. Hagedorn, S.G. Satterfield, Three-dimensional shape analysis of coarse aggregates: new techniques for and preliminary results on several different coarse aggregates and reference rocks, Cement Concr. Res. 36 (2006) 1619–1627.
[26] E.J. Garboczi, J.W. Bullard, Contact function, uniform-thickness shell volume, and convexity measure for 3D star-shaped random particles, Powder Technol. 237 (2013) 191–201, https://doi.org/10.1016/j.powtec.2013.01.019.

[27] J.W. Bullard, E.J. Garboczi, Defining shape measures for 3D star-shaped particles: Sphericity, roundness, and dimensions, Powder Technol. 249 (2013) 241–252.
[28] X. Jia, E.J. Garboczi, Advances in shape measurement in the digital world, Particuology 26 (2016) 19–31.
[29] E.J. Garboczi, K.A. Riding, Mohammadreza Mirzahosseini, Particle shape effects on particle size measurement for crushed waste glass, Adv. Powder Technol. 28 (2017) 648–657.
[30] COIN Project report no 13, Low porosity through optimized particle packing of concrete matrix, COIN P1 Advanced cementing materials and admixtures, SP 1.5 Low porosity/permeability, (2009).
[31] H.H.C. Wong, A.K.H. Kwan, Packing density: a key concept for mix design of high performance concrete, Proceedings of the Materials Science and Technology in Engineering Conference, HKIE Materials Division, Hong Kong, 2005, pp. 1–15.
[32] ASTM C128: Standard Test Method for Density, Relative Density (Specific Gravity), and Absorption of Fine Aggregate.
[33] Handbook of Rock Excavation, Methods and Cost, Halbert Powers Gillette, 1916.
[34] Foundation Engineering Handbook, Hsai-Yang Fang, CRC Press, 2013.
[35] J.M.R. Fernlund, The effect of particle form on sieve analysis: a test by image analysis, Eng. Geol. 50 (1998) 111–124.
[36] C.F. Mora, A.K.H. Kwan, H.C. Chan, Particle size distribution analysis of coarse aggregate using digital image processing, Cement Concr. Res. 28 (6) (1998) 921–932.
[37] D. Moore, ý G.P. McCabe, Introduction to the Practice of Statistics, W.H. Freeman, 9780716796572, 2002.
[38] S.T. Erdoğan, D.W. Fowler, E.J. Garboczi, Shape and size of microfine aggregates: X-ray microcomputed tomography vs. laser diffraction, Powder Technol. 177 (2007) 53–63.
[39] H.H.C. Wong, A.K.H. Kwan, Packing density of cementitious materials: part 1 -measurement using a wet packing method, Mater. Struct. 41 (2008) 689–701 https://doi.org/10.1617/s11527-007-9274-5.
[40] R.P. Zou, A.B. Yu, Evaluation of the packing characteristics of mono-sized non-spherical particles, Powder Technol. 88 (1) (1996) 71–79.
[41] A.K.H. Kwan, C.F. Mora, Effects of various shape parameters on packing of aggregate particles, Mag. Concr. Res. 53 (2) (2001) 91–100.
[42] Jiong Hua, Kejin Wang, Effect of coarse aggregate characteristics on concrete rheology, Constr. Build. Mater. 25 (3) (2011) 1196–1204.
[43] BS EN 1015-6: Methods of test for mortar for masonry — Part 6: Determination of bulk density of fresh mortar.